Modeling and inverse feedforward control for conducting polymer actuators with hysteresis

Modeling and inverse feedforward control for conducting polymer actuators with hysteresis

Xiangjiang Wang[1,2], Gursel Alici[2] and Xiaobo Tan[3]

[1] School of Mechanical Engineering, University of South China, Hengyang 421001,
People's Republic of China
[2] School of Mechanical, Materials and Mechatronic Engineering, University of Wollongong, 2522 NSW,
Australia
[3] Department of Electrical and Computer Engineering, Michigan State University, East Lansing,
MI 48824, USA

E-mail: gursel@uow.edu.au

Abstract

Conducting polymer actuators are biocompatible with a small footprint, and operate in air or liquid media under low actuation voltages. This makes them excellent actuators for macro- and micro-manipulation devices, however, their positioning ability or accuracy is adversely affected by their hysteresis non-linearity under open-loop control strategies. In this paper, we establish a hysteresis model for conducting polymer actuators, based on a rate-independent hysteresis model known as the Duhem model. The hysteresis model is experimentally identified and integrated with the linear dynamics of the actuator. This combined model is inverted to control the displacement of the tri-layer actuators considered in this study, without using any external feedback. The inversion requires an inverse hysteresis model which was experimentally identified using an inverse neural network model. Experimental results show that the position tracking errors are reduced by more than 50% when the hysteresis inverse model is incorporated into an inversion-based feedforward controller, indicating the potential of the proposed method in enabling wider use of such smart actuators.

Keywords: conducting polymer actuators, hysteresis model, Duhem model, system identification, inversion-based feedforward control

(Some figures may appear in colour only in the online journal)

1. Introduction

Conducting polymer actuators have received significant attention [1–4] in the past decade due to their low operating voltage, inherent biocompatibility, high force output to weight ratio, noiseless operation with a small footprint, and insensitivity to magnetic fields. These actuators could be engineered as bending actuators like a cantilever beam, which are suitable for activating micro-pumps, micro-switches, micro-grippers and micro-cantilevers, to move, position or hold microdevices and objects, and manipulate biological samples. Mathematical models have previously been developed to understand their quasi-static and dynamic behaviors and to establish feedback control strategies [5–7]. Feedback control and open-loop control (using an inverse model of the actuator) techniques can be employed to control the actuator's bending displacement or bending angle [8–10]. In particular, open-loop control techniques are desirable for such smart actuators since it is not practical to use an external sensor for feedback in most of the applications envisioned. With this in mind, it is crucial to model non-linear effects such as hysteresis to enhance the accuracy of the actuator model

and hence increase the positioning ability of these actuators without using an external sensor.

When conducting polymer actuators are influenced by their hysteresis non-linearity, the whole system usually exhibits undesirable inaccuracies. The hysteresis phenomenon occurs in almost all smart material-based actuators [11–15]. Researchers have proposed various methods for hysteresis modeling, however, hysteresis modeling has not been reported for tri-layer conducting polymer actuators. The Preisach model and various other hysteresis models are widely used [16–18], but these operators are typically difficult to identify and invert [19, 20]. On the other hand, the Duhem hysteresis model is simpler to construct and experimentally identify [21, 28]. Over the years, various control techniques have been developed to mitigate the effects of hysteresis. Much of this renewed interest is a direct consequence of the importance of smart materials in numerous current applications. The interest in studying dynamic systems with actuator hysteresis is also motivated by the fact that they are non-linear systems with non-smooth non-linearities for which traditional control methods are insufficient and thus require the development of alternative approaches.

In this paper, we develop a method for building a hysteresis model for tri-layer conducting polymer actuators. The model consists of two sub-systems, a rate-independent Duhem hysteresis model and a linear dynamic model. The efficacy of the model is demonstrated with experimental results obtained from the actuators controlled through an inversion-based feedforward controller. It must be noted the success of the feedforward control depends on the accuracy of the mathematical model describing the dynamic behavior of the actuators. As reported before [5, 10, 23, 24, 29], it is virtually impossible to have a mathematical model accounting for a wide range of frequencies and the variations in the electrical, chemical and mechanical parameters of these tri-layer actuators including their non-linear behavior such as creep and hysteresis. We have previously reported on a hysteresis model to be used in the feedforward control of these actuators [28], and other smart actuators whose dynamic behavior and hysteretic behavior can similarly be modeled and identified, and subsequently it can be used in a feedforward controller in order to control the displacement output of these actuators. This paper incorporates this hysteresis model into the linear model of the actuator to establish a more accurate mathematical model, for the sensorless position control of these actuators.

2. Experimental set-up

Figure 1 shows the structure of the bending-type tri-layer polymer actuators considered in this study. It consists of two outer polypyrrole (PPy) layers that are the active components (serving as electrodes), an inner porous separator of PVDF that holds the liquid electrolyte, and two sputter-coated gold layers with negligible thickness for electrochemically growing the polymer layers on the PVDF layer. The bending actuator with the desired length and width is cut from the bulk sheet. This composite structure exhibits a simple bending motion

Figure 1. Geometry of the conducting polymer actuator.

like a bi-layer cantilever. When a potential difference or current is passed between the polymer (PPy) electrodes via the clamp, the polymer actuator bends and outputs a mechanical motion at its tip, due to an electrochemical reaction. We have presented the procedure for the synthesis of the actuators in our previous study [22]. Such bending actuators are suitable for moving, positioning or holding microdevices, objects and biological samples. In particular, due to their compliance, they can be used as a cell-tapper to mechanically stimulate a single cell [25, 26].

Figure 2 shows the experimental set-up for model identification and control. The input voltage applied to the actuator is first generated by the software and then transmitted to an NI USB-6251 DAQ board and to an eDAQ potentiostat (eDAQ, model EA161) operating in the two-electrode mode. A non-contact laser sensor (Micro-epsilon, model NCDT-1700-10) is used to measure the tip displacement of the actuator. The data is sent to the computer via a data logger (e-Corder, model ED821). The control system is built in MATLAB which is connected to the experimental hardware through object linking.

It is usually difficult to build accurate analytical or physical models due to non-linearities and multi-physics (electro-chemo-mechanical) phenomena associated with the actuator. It is feasible, however, to build a system model empirically that is adequate for control system design, analysis, and implementation.

3. Actuator model

To identify the mathematical model of a tri-layer PPy actuator, several sinusoidal voltages were applied to a 15 mm-long, 5 mm-wide, 0.17 mm-thick actuator. The input voltage signal of $u(t) = \sin(\omega t)$, with a range of frequencies, ω (rad s^{-1}) = 0.5π, 1.0π, and 2.0π, was chosen. The relationship between the input voltage and output displacement $y(t)$ can be used to obtain a transfer function model of the actuator.

3.1. Identifying the discrete-time transfer function

By ignoring non-linearities [10], the actuator can be first modeled as a linear system which can be represented by a discrete-time transfer function $G_1(z)$ shown in figure 3. Considering the relationship between the input $u(k)$ and output $y(k)$ to be a 'black box', one can experimentally identify the transfer function in a straightforward manner.

We can employ offline identification techniques to identify the discrete-time transfer function. Here a least-square estimation method is used. As we reported previously [8, 10, 23, 24], although the dynamics of conducting polymer
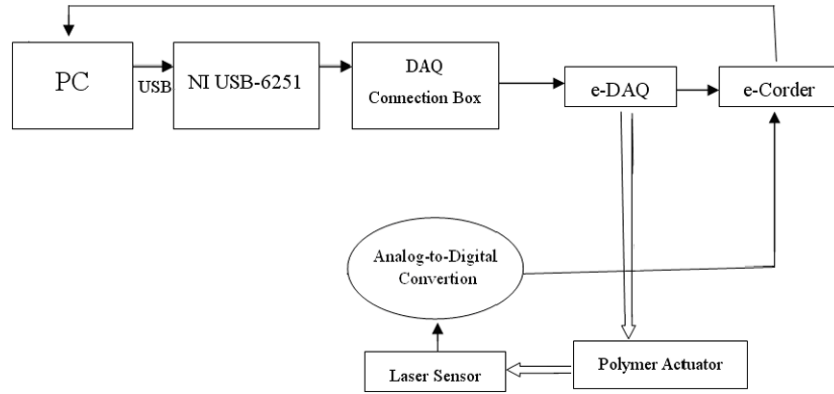
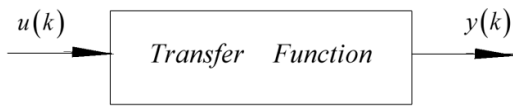**Figure 2.** Schematic representation of the experimental set-up.

Figure 3. Transfer function representation of the actuator.

Table 1. The numerical values of the model parameters of equation (1).

b_{10}	b_{11}	a_{11}	a_{12}
0.0352	−0.0318	−1.0831	0.0859

actuators is of high order, it can be approximated with a second-order system,

$$G_1(z) = \frac{b_{10}z + b_{11}}{z^2 + a_{11}z + a_{12}}. \tag{1}$$

Equation (1) implies

$$A(z)y(t) = B(z)u(t). \tag{2}$$

With $A(z) = 1 + a_{11}z^{-1} + a_{12}z^{-2}$

$$B(z) = b_{10}z^{-1} + b_{11}z^{-2}.$$

The term z^{-1} is the unit delay operator, and $z^{-1}y(t) = y(t-1)$.

We employ the least-square method to identify the parameters of the actuator system. The parameter vector θ is defined as

$$\theta^{\mathrm{T}} = [a_{11}, a_{12}; b_{10}, b_{11}]. \tag{3}$$

The regression vector is described as

$$\varphi^{\mathrm{T}}(t) = [-y(t-1), -y(t-2); u(t-1), u(t-2)]. \tag{4}$$

Equation (1) can be written as

$$y_t = H_t\theta \tag{5}$$

with

$$y_t = \begin{bmatrix} y(1) \\ y(2) \\ \vdots \\ y(t) \end{bmatrix}, \qquad H_t = \begin{bmatrix} \varphi^{\mathrm{T}}(1) \\ \varphi^{\mathrm{T}}(2) \\ \vdots \\ \varphi^{\mathrm{T}}(t) \end{bmatrix}.$$

According to the least squares criterion, the estimated value of parameter vector θ is

$$\hat{\theta} = (H_t^{\mathrm{T}}H_t)^{-1}H_t^{\mathrm{T}}y_t. \tag{6}$$

This linear model can be used to simulate the bending displacement under a voltage input. The model identification errors are shown in figure 4. The error $e(t)$ is the error between the real output $y(t)$ and the predicted output $y_1(t)$. We see that the output predicted through the linear transfer function model deviates significantly from the experimental output. One reason for modeling errors is the unmodeled non-linearities such as the hysteresis, generally neglected in previously reported models.

The dynamics of conducting polymer actuators can accurately be represented by a high model (at least fourth order, [10, 24]) for an acceptable bandwidth ($\sim$38 Hz). The numerical values of the parameters for the second-order model in equation (1) are experimentally identified and provided in table 1. It must also be noted that the magnitude of the input displacement is kept low such that the actuator can show a linear dynamic behavior [8, 10], which can be identified by using linear system modeling and identification techniques.

3.2. The hysteresis model incorporated into the actuator model

To improve the accuracy of the actuator model, the influence of the hysteresis non-linearity needs to be modeled. We consider a transfer function $G_2(z)$ connected in cascade to a hysteresis model $H(t)$, as shown in figure 5.

The time shift between the fundamental frequency component of the displacement output $y(t)$ and the input voltage $u(t)$ is Δt, which is determined by comparing the peaks of the experimental displacement signal and the input voltage. To eliminate the effect of the phase shift introduced by the transfer function, the input signal needs to be given a backward phase shift [27]; in this case, the phase shift will be of $\varphi(\omega) = \omega\Delta t$, which results in the input for the hysteresis model

$$v(t) = \sin(\omega t - \omega\Delta t). \tag{7}$$

(a)

(b)

(c)
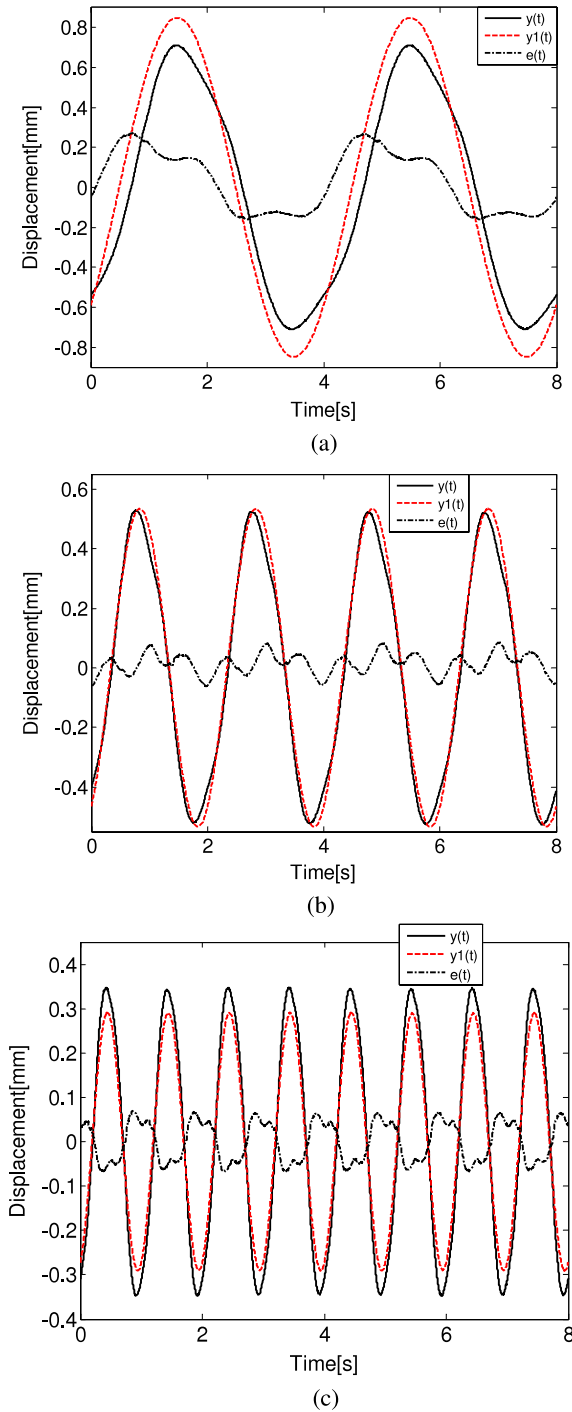
Figure 4. Comparison of the predicted actuator displacement output with the experimental displacement output under sinusoidal inputs with different frequencies. (a) Input $u(t) = \sin(0.5\pi t)$. (b) Input $u(t) = \sin(\pi t)$. (c) Input $u(t) = \sin(2\pi t)$.

Note that, with (7), one ensures the output of the hysteresis reaches maximum (minimum, resp.) when the input reaches maximum (minimum, resp.), which is a necessary condition for a rate-independent, monotonic hysteresis operator. Also, to eliminate the frequency-dependent amplitude property of the linear part, the output data is normalized as follows:

$$w(t) = \frac{y(t)}{k} \qquad (8)$$
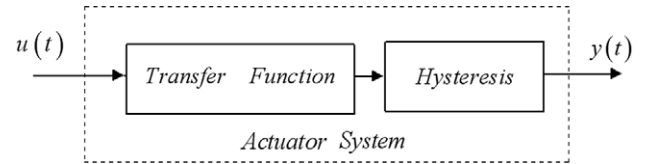
Figure 5. The block diagram of the actuator containing hysteresis non-linearities.
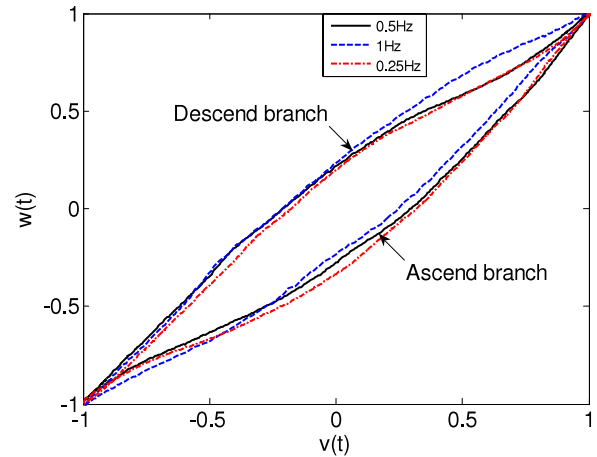
Figure 6. Hysteresis loops of the actuator under different input frequencies.

where $k = \max(|y(t)|)$. With (8), we ensure that the output $w(t)$ of the hysteresis has the same range (namely $[-1, 1]$ in this case) when its input is of different frequencies but of the same amplitude, which is a necessary condition for the rate-independent hysteresis model.

After adjusting the input and output signals, the hysteresis curves are obtained as shown in figure 6, where $v(t)$ is the input signal and $w(t)$ is the output signal. The hysteresis curves are frequency or rate-independent as they show very similar hysteresis behavior under different input frequencies. The discrepancy between the hysteresis loops in figure 6 is negligibly small.

The hysteresis phenomenon occurs in almost all the smart material-based actuators, such as piezoceramics, MR and magnetostrictive materials. With this non-linearity, the whole system usually exhibits undesirable inaccuracies, oscillations or even instability. Over many years, various control techniques had been developed to mitigate the effects of hysteresis and recently these have again attracted significant attention from both industry and academic research. Much of this renewed interest is a direct consequence of the importance of hysteresis in numerous applications.

3.2.1. Modeling the hysteresis. We employ the Duhem hysteresis model to mathematically represent the hysteresis loops in figure 6. The generalized Duhem model is given by [21, 28]

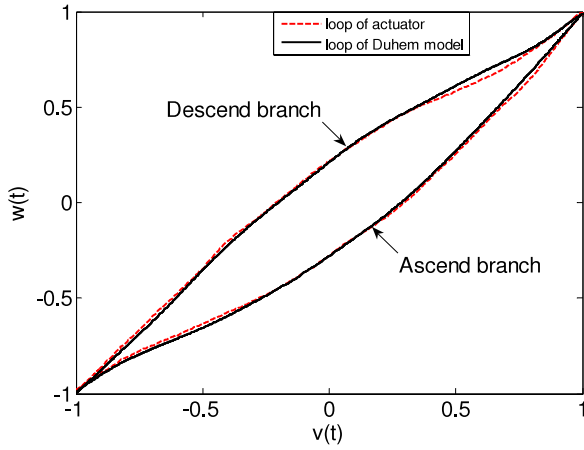$$\frac{dw}{dt} = \alpha \left| \frac{dv}{dt} \right| [f(v) - w] + \frac{dv}{dt} g(v) \qquad (9)$$

4

Figure 7. Hysteresis loop of Duhem model.

where $f(v)$ and $g(v)$ are the characteristic functions of the hysteresis mode, $v(t)$ is the input signal, and $w(t)$ is the output signal. Equation (9) can also be written as

$$\frac{dw_A}{dv} = \alpha[f(v) - w_A] + g(v), \qquad \dot{v} > 0 \qquad (10)$$

$$\frac{dw_D}{dv} = -\alpha[f(v) - w_D] + g(v), \qquad \dot{v} < 0 \qquad (11)$$

where $w_A(t)$ and $w_D(t)$ are the mathematical functions describing the ascending and descending branches, respectively. It follows that the characteristic functions are obtained as

$$f(v) = \frac{1}{2}(w_A + w_D) + \frac{1}{2\alpha}\left(\frac{dw_A}{dv} - \frac{dw_D}{dv}\right) \qquad (12)$$

$$g(v) = \frac{1}{2}\left(\frac{dw_A}{dv} + \frac{dw_D}{dv}\right) + \frac{1}{2}\alpha(w_A - w_D). \qquad (13)$$

Based on equations (12) and (13), the functions $f(v)$ and $g(v)$ in the Duhem model can be identified from a set of experiment data. $w_A(t)$ and $w_D(t)$ as well as their derivatives are needed to identify $f(v)$ and $g(v)$.

In equations (9)–(13), α, which is a positive number, can be regarded as a weighting factor. When identifying $f(v)$ and $g(v)$, a larger error arises in the evaluation of the derivative curves than in the ascending or descending branches of the hysteresis loop. With this in mind, a large value of $\alpha = 80$ is selected to minimize the entire identification error. A neural network is employed to improve the accuracy of the identification functions $f(v)$ and $g(v)$, and to identify the ascending branch $w_A(t)$ and the descending branch $w_D(t)$ as shown in figure 6.

The neural network identification method is used to build $f(v)$ and $g(v)$. The hysteresis curves shown in figure 7 are the simulated results calculated from the Duhem hysteresis model of equation (9), which is close to the experimental results shown in figure 6 (0.5 Hz). It leads to the conclusion that the hysteresis modeling method is effective in representing the hysteresis of the conducting polymer actuators considered in this study.

Table 2. The numerical values of the model parameters in equation (19).

b_{20}	b_{21}	a_{21}	a_{22}
0.0976	-0.0922	-0.6491	-0.3453

3.2.2. Building the transfer function of the linear part for a non-linear system. In order to compensate for the hysteresis effect in the actuator, represented by the block diagram in figure 5, the hysteresis inverse model must be established and experimentally identified. The Duhem hysteresis inverse model can be expressed as

$$\frac{dq(t)}{dt} = \alpha \left|\frac{dw}{dt}\right| [F(w) - q(t)] + \frac{dw}{dt}G(w) \qquad (14)$$

where $F(w)$ and $G(w)$ are the characteristic functions of the hysteresis inverse model, and $q(t)$ is the inverse function of $w(t)$. In figure 6, the ascending branch $w_A(t)$ and the descending branch $w_D(t)$ are monotonic, so they are reversible. This suggests that equation (14) can be re-written as

$$\frac{dq_A}{dw} = \alpha[F(w) - q_A] + G(w), \qquad \dot{w} > 0 \qquad (15)$$

$$\frac{dq_D}{dw} = -\alpha[F(w) - q_D] + G(w), \qquad \dot{w} < 0 \qquad (16)$$

where $q_A(t)$ is the inverse function of $w_A(t)$ and $q_D(t)$ is the inverse function of $w_D(t)$. From equations (15) and (16), we obtain the characteristic functions,

$$F(w) = \frac{1}{2}(q_A + q_D) + \frac{1}{2\alpha}\left(\frac{dq_A}{dw} - \frac{dq_D}{dw}\right) \qquad (17)$$

$$G(w) = \frac{1}{2}\left(\frac{dq_A}{dw} + \frac{dq_D}{dw}\right) + \frac{1}{2}\alpha(q_A - q_D). \qquad (18)$$
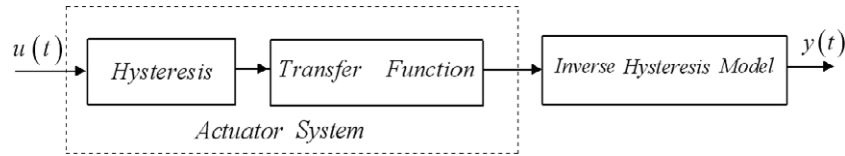
Similarly, $F(w)$ and $G(w)$ can be estimated using the inverse neural network model. The transfer function $G_2(z)$ of the non-linear system can be identified according to figure 8. It must be noted that the hysteresis inverse model must be obtained in order to negate the hysteresis non-linearities in the real system—the actuator, as shown in figure 8.

The discrete transfer function of the actuator is described by

$$G_2(z) = \frac{b_{20}z + b_{21}}{z^2 + a_{21}z + a_{22}}. \qquad (19)$$

As shown in figure 5, the transfer function given by equation (19) is cascaded with the Duhem hysteresis model to obtain the actuator model. Figure 9 shows the results of the hysteresis system model identification errors: $e(t)$ is the error between the real actuator output $y(t)$ and the actuator system hysteresis model output $y_h(t)$. The numerical values of the parameters in our experimentally identified model are presented in table 2.

To demonstrate the significance of a hysteresis model, the actuator output is calculated according to the block diagram in

Figure 8. The block diagram of the actuator and the inverse hysteresis model to obtain a transfer function of the linear part for the actuator.
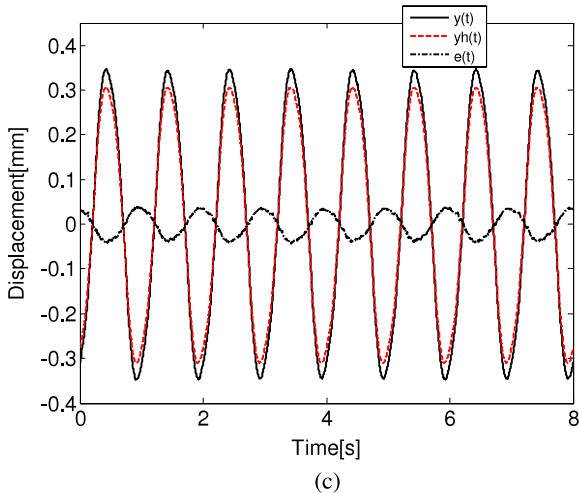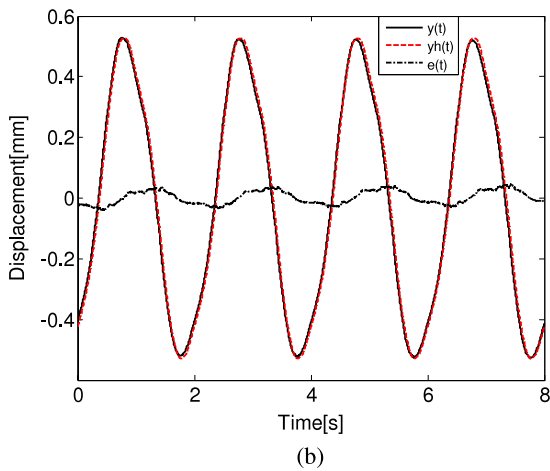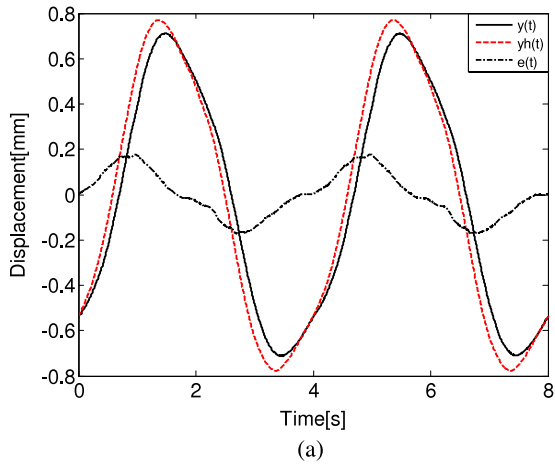
Table 3. The RMS errors of $u(t) = \sin(\omega t)$.

ω	0.5π	1π	2π
RMS errors of linear model	0.1528	0.0371	0.0451
RMS errors of non-linear model	0.1026	0.0224	0.0262

figure 8, where the hysteresis model is negated by the inverse hysteresis model in order to obtain a linear transfer function. The position tracking root-mean-square (RMS) errors of these two models (with a hysteresis model and without a hysteresis model) are calculated from equation (20) and shown in table 3.

$$\text{RMS} = \sqrt{\frac{1}{m}\sum_{i=1}^{m}(y_i - y_{\text{d}i})^2}. \qquad (20)$$

With reference to the results in table 3, the hysteresis model has improved the accuracy of the actuator model significantly. The RMS errors of the actuator model including hysteresis model are much smaller than those of the linear model. It follows that the proposed hysteresis modeling approach is effective. We postulate that the linear dynamics represent the electrical dynamics and the viscoelastic dynamics, while the hysteresis captures the non-linear relationship between the stress output and the strain change induced by ion transport in and out of the PPy layers.

4. Inversion-based feedforward control: controlling actuator output without using feedback data

For a given conducting polymer actuator, $y_{\text{d}}(t)$ is the desired input and $y(t)$ is the real output. A desired input can be realized if the inverse actuator model compensates for the actuator dynamics and non-linearities. The two different actuator models obtained in section 3 will be used to develop the inverse model for the feedforward control system.

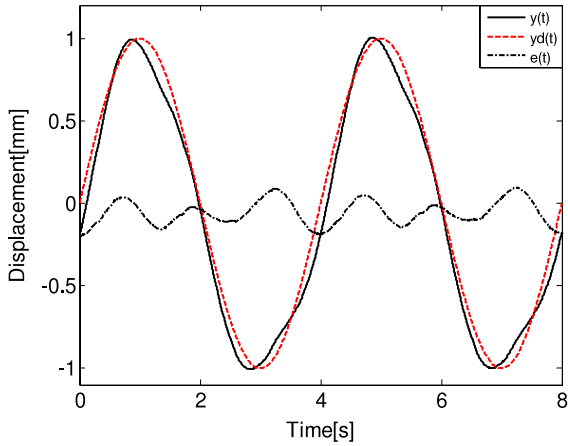### 4.1. Linear inverse model feedforward control

Figure 10 shows the schematic of the linear inverse model $G_1^{-1}(z)$ feedforward controller. This model does not contain the hysteresis model. The output is given by

$$y(t) = y_{\text{d}}(t)G_1^{-1}(z)G_1(z). \qquad (21)$$

The desired output is $y_{\text{d}}(t) = \sin(\omega t)$, with a range of frequencies, ω (rad s^{-1}) $= 0.5\pi$, 1.0π, and 2.0π. Based on the desired displacement, the actuator voltage signals are

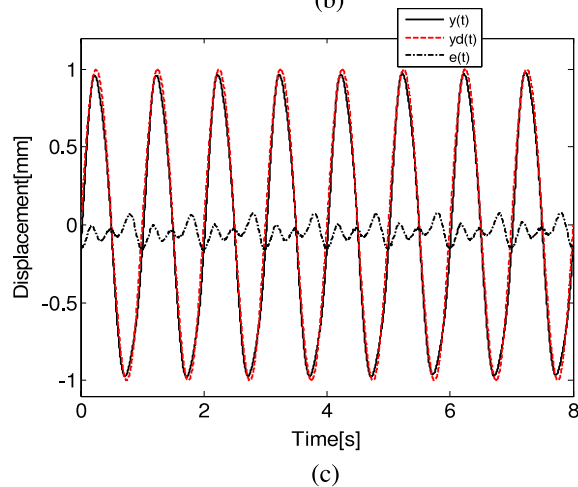**Figure 9.** Comparison of the actuator + hysteresis model output and the experimental actuator output under different frequencies. (a) Input $u(t) = \sin(0.5\pi t)$. (b) Input $u(t) = \sin(\pi t)$. (c) Input $u(t) = \sin(2\pi t)$.

Figure 10. Schematic of the linear inverse model for the feedforward controller.
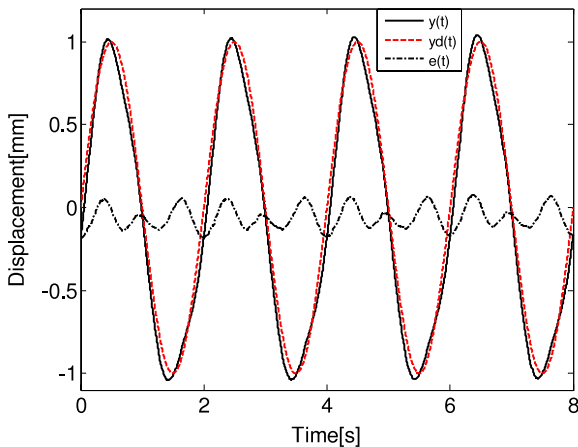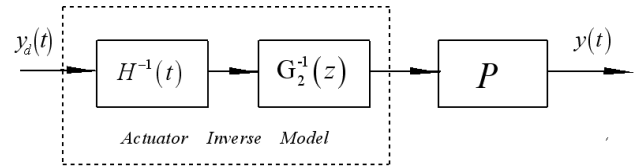
Figure 12. Schematic of the hysteresis inverse model for the feedforward controller.

Table 4. The RMS errors of $y_d(t) = \sin(\omega t)$.

ω	0.5π	1π	2π
RMS errors of linear inverse model control	0.0933	0.0898	0.0731
RMS errors of hysteresis inverse model control	0.0417	0.0390	0.0344

calculated from the inverse model. Figure 11 shows the real output $y(t)$ of the actuator, the desired output $y_d(t)$ and the associated tracking errors $e(t)$.

4.2. Hysteresis inverse model feedforward control

In order to control the actuator system with hysteresis, a hysteresis inverse model $H^{-1}(t)$ cascades the inverse plant model $G_2^{-1}(z)$ to obtain the actuator inverse model. The schematic of this inverse model feedforward controller is shown in figure 12. The output is given by

$$y(t) = y_d(t)H^{-1}(t)G_2^{-1}(z)G_2(z)H(t). \qquad (22)$$

The desired output is $y_d(t) = \sin(\omega t)$, with a range of frequencies, ω (rad s^{-1}) $= 0.5\pi$, 1.0π, and 2.0π. Figure 13 shows the real output $y(t)$ of the actuator, the desired output $y_d(t)$ and the associated tracking error $e(t)$. The comparison of the RMS errors of the two inverse model feedforward controllers is shown in table 4.

Compared with the linear inverse model control results, the performance of the inverse model control based on the proposed hysteresis model is better. The results show that the tracking errors are reduced by at least 50% if the hysteresis inverse model compensation is added to the feedforward controller. These results further demonstrate that the hysteresis modeling approach based on the Duhem hysteresis model is effective for obtaining a reasonably accurate hysteresis model, and therefore an actuator model.

5. Conclusions

We have employed identification techniques to establish the discrete-time transfer function models for tri-layer conducting polymer actuators which can operate both in dry and wet media, but the accuracy of such linear models is limited due to unmodeled non-linearities. A linear transfer function in cascade with the Duhem hysteresis model has been successfully used to generate a non-linear model of the actuator which has improved the command tracking
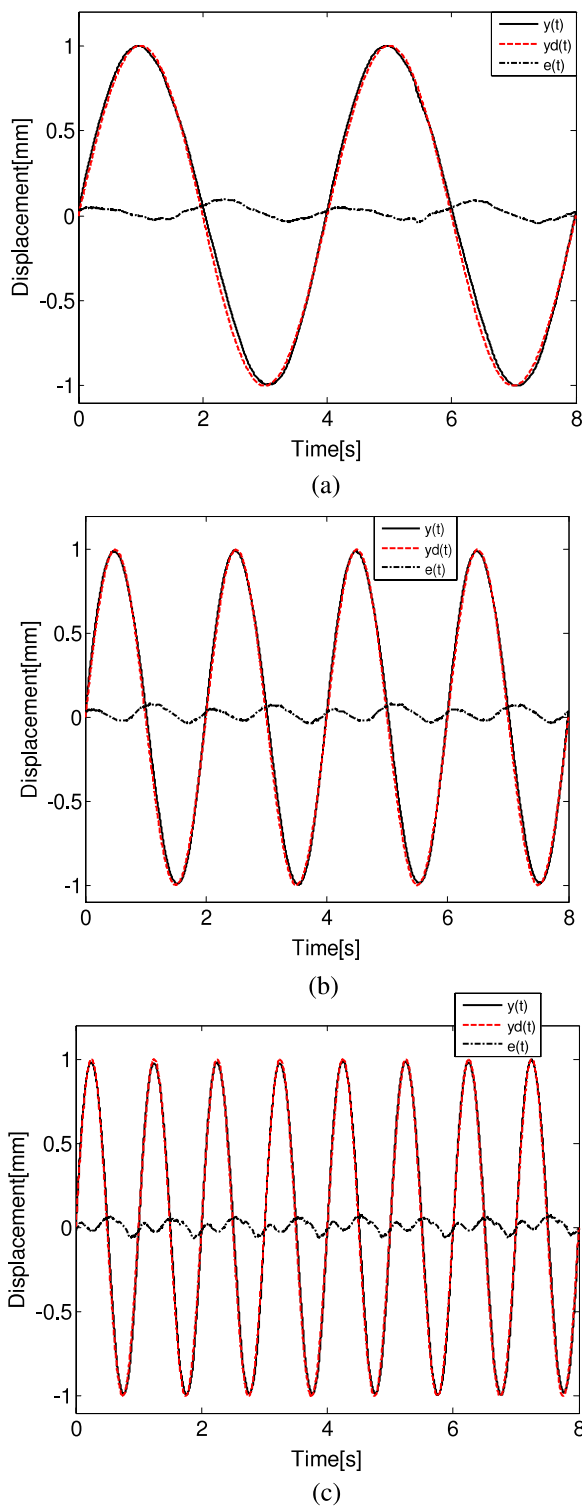

Figure 11. The real actuator output under the inverse model feedforward controller and associated tracking errors. (a) Input $y_d(t) = \sin(0.5\pi t)$. (b) Input $y_d(t) = \sin(\pi t)$. (c) Input $y_d(t) = \sin(2\pi t)$.

(a)

(b)

(c)

Figure 13. The real actuator output under the hysteresis inverse model feedforward controller and associated tracking errors. (a) Input $y_d(t) = \sin(0.5\pi t)$. (b) Input $y_d(t) = \sin(\pi t)$. (c) Input $y_d(t) = \sin(2\pi t)$.

performance of the actuators. The performance of the model including the hysteresis model was tested against the linear model. The experimental results presented show that improved performance can be obtained under different frequencies. It should be noted that after a long operation time

(>2 h), the solvent evaporation can significantly change the performance of the actuator, as reported in [10]. With this in mind, the proposed inversion-based feedforward method will not function satisfactorily over extended periods of time unless the actuator is encapsulated to make sure that solvent evaporation does not occur. Otherwise, operation-time-dependent dynamic models should be identified and, depending on the duration of the operation, a suitable dynamic model should be used in the feedforward controller.

Based on two identified actuator models, we implemented inversion-based feedforward control strategies and compared their tracking errors. The experimental results presented demonstrate that the hysteresis inverse model feedforward controller is the more successful control strategy. Comparing the tracking results in [24] (in particular, figures 18 and 19 in [24]) with those in the current work, one can see that the (open-loop) feedforward control used in this paper results in significantly lower errors. Specifically, the maximum tracking errors reported in this paper are about 5% of the amplitudes of the reference trajectories, while the maximum errors reported in [24] are 15–20% of the amplitudes of the references. This comparison shows the importance of capturing the hysteresis non-linearity in the model. The strength of the approach in [24], however, is that the (linear) model there incorporates material physics, while the linear dynamics in this work is an empirical model. A promising direction for future work, therefore, is to merge the hysteresis model presented in this work with the physics-based model in [24].

The hysteresis inverse model feedforward control strategy will help widen the implementation of smart-materials-based actuators like electroactive polymer actuators in new real-world applications where external sensory feedback is impossible or costly.

Acknowledgments

References

[1] Han G and Shi G 2004 Conducting polymer electrochemical actuator made of high-strength three-layered composite films of polythiophene and polypyrrole *Sensors Actuators* B **99** 525–31

[2] Gaihre B, Alici G, Spinks G M and Cairney J M 2011 Synthesis and performance evaluation of thin film PPy-PVDF multilayer electroactive polymer actuators *Sensors Actuators* A **165** 321–8

[3] Hiraoka M, Fiorini P, O'Callaghan J, Yamashita I, Van Hoof C and Op de Beeck M 2012 Miniature conductive polymer actuators for high pressure generation in lab on chip systems *Sensors Actuators* A **177** 23–9

[4] Fuchiwaki M, Tanaka K and Kaneto K 2009 Planate conducting polymer actuator based on polypyrrole and its application *Sensors Actuators* A **150** 272–6

[5] Shoa T, Yoo D S, Walus K, David J and Madden W 2011 A dynamic electromechanical model for electrochemically driven conducting polymer actuators *IEEE/ASME Trans. Mechatronics* **16** 42–9

[6] Alici G 2009 An effective modelling approach to estimate nonlinear bending behaviour of cantilever type conducting polymer actuators *Sensors Actuators* B **141** 284–92

[7] Du P, Lin X and Zhang X 2010 A multilayer bending model for conducting polymer actuators *Sensors Actuators* A **163** 240–6

[8] John S W, Alici G and Cook C D 2010 Inversion-based feedforward control of polypyrrole trilayer bender actuators *IEEE/ASME Trans. Mechatronics* **15** 149–56

[9] Yao Q, Alici G and Spinks G M 2008 Feedback control of tri-layer polymer actuators to improve their positioning ability and speed of response *Sensors Actuators* A **144** 176–84

[10] Fang Y, Tan X and Alici G 2008 Robust adaptive control of conjugated polymer actuators *IEEE Trans. Control Syst. Technol.* **16** 600–12

[11] Stepanenko Y and Su C Yi 1998 Intelligent control of piezoelectric actuators *Proc. 37th IEEE Conf. on Decision & Control* pp 4234–9

[12] Ru C H and Sun L N 2005 Hysteresis and creep compensation for piezoelectric actuator in open-loop operation *Sensors Actuators* A **122** 124–30

[13] Chen L W, Lin C Y and Wang C C 2002 Dynamic stability analysis and control of a composite beam with piezoelectric layers *Compos. Struct.* **56** 97–109

[14] Davino D, Natale C, Pirozzi S and Visone C 2005 A fast compensation algorithm for real-time control of magnetostrictive actuators *J. Magn. Magn. Mater.* **290/291** 1351–4

[15] Iyer R and Tan X 2009 Control of hysteretic systems through inverse compensation: inversion algorithms, adaptation, and embedded implementation *IEEE Control Syst. Mag.* **29** 83–99

[16] Zhou J, Wen C and Zhang Y 2004 Adaptive backstepping control of a class of uncertain nonlinear systems with unknown backlash-like hysteresis *IEEE Trans. Autom. Control* **49** 1751–7

[17] Su C Y, Wang Q, Chen X and Rakheja S 2005 Adaptive variable structure control of a class of nonlinear systems with unknown Prandtl–Ishlinskii hysteresis *IEEE Trans. Autom. Control* **50** 2069–74

[18] Zhou X F, Yang S X, Qi G N and Hu X P 2005 Tracking control of piezoceramic actuators by using Preisach model *ICMIT 2005: Control Systems and Robotics* vol 6042, p 604248

[19] Ping G E and Jouaneh M 1997 Generalized Preisach model for hysteresis nonlinearity of piezoceramic actuators *Precis. Eng.* **20** 99–111

[20] Dubra A, Massa J S and Paterson C 2005 Hysteresis compensation in PZT bimorph mirrors Preisach's classical and nonlinear models *5th Int. Workshop on Adaptive Optics for Industry and Medicine* vol 6018, p 60181E

[21] Wang X S, Hong H and Su C Yi 2003 Adaptive robust control of dynamic systems with unknown input hysteresis *ICCA'03: The 4th Int. Conf. on Control and TuAO54 Automation* pp 138–42

[22] Wu Y, Alici G, Spinks G M and Wallace G G 2006 Fast trilayer polypyrrole bending actuators for high speed applications *Synth. Met.* **156** 1017–22

[23] Wang X, Alici G and Nguyen C H 2013 Adaptive sliding mode control of tri-layer conjugated polymer actuators *Smart Mater. Struct.* **22** 025004

[24] Nguyen C H, Alici G and Wallace G G 2012 Modelling trilayer conjugated polymer actuators for their sensorless position control *Sensors Actuators* A **185** 82–91

[25] Gaihre B, Alici G, Spinks G M and Cairney J M 2012 Pushing the limits for microactuators based on electroactive polymers *IEEE/ASME J. Microelectromech. Syst.* **21** 574–85

[26] Alici G, Devaud V, Renaud P and Spinks G M 2009 Conducting polymer microactuators operating in air *J. Micromech. Microeng.* **19** 025017

[27] Wang X S, Mao Y, Wang X J and Su C 2007 Adaptive variable structure control of hysteresis in GMM actuators based on Prandtl–Ishlinskii model *33rd Annual Conf. on the IEEE Industrial Electronics Society (IECON) (Taipei, Nov.)* pp 721–6

[28] Wang X, Alici G and Nguyen C 2013 A methodology to establish a hysteresis model for trilayer conducting polymer actuators *2013 IEEE/ASME Int. Conf. on Advanced Intelligent Mechatronics (Wollongong, July)* pp 111–6

[29] Nguyen C H, Alici G and Wallace G G 2013 An advanced mathematical model and its experimental verification for tri-layer conjugated polymer actuators *IEEE/ASME Trans. Mechatronics* doi:10.1109/TMECH.2013.2280012